Abdominal injury assessment using THOR prototype abdomen

Contents

4.1 Introduction

Impactor or seatbelt loading tests on PMHS provide global response data in terms of force and penetration as well as injury outcomes but do not allow to estimate the loading severity for a specified organ. Human finite element models allow to reproduce these loadings while looking at detailed engineering parameters at the organ level. In order to find an injury criterion applicable to the IFSTTAR / Toyota prototype abdomen, PMHS studies were reproduced with the THUMS finite element human model. The injury outcomes from the PMHS studies in parallel with the organ loading parameters from the model would allow to set a threshold for the pressure measured by the APTS in the prototype abdomen in order to define an injury criterion.

4.2 Reproduction of PMHS tests with the THUMS model

4.2.1 Presentation of the THUMS model

The THUMS model is a full body human finite element model developed under LS-DYNA by Toyota Motor Corporation and Toyota Central R & D Labs., Inc.. The last commercial version of the model is version 4.0 as described in Shigeta et al. 2009. This model have proportions close to an average adult male (size 179 cm, weight 74 kg according to THUMS Manual (Toyota Motor Corporation 2011). The thorax and abdomen of the version 4.0 model have been created using CT [1] scans from a 39 year-old subject (size 173 cm, weight 77 kg). The scans were from the University of Michigan database. The model is available in two different positions. The model in the pedestrian (standing) position was directly build from the scans. The model in car occupant position was derived from the pedestrian model. Figure 4.1 shows the two commercial models. Models specifically positioned to reproduce PMHS tests from the literature received from Toyota Motor Corporation have been used for impactor and seatbelt simulations.

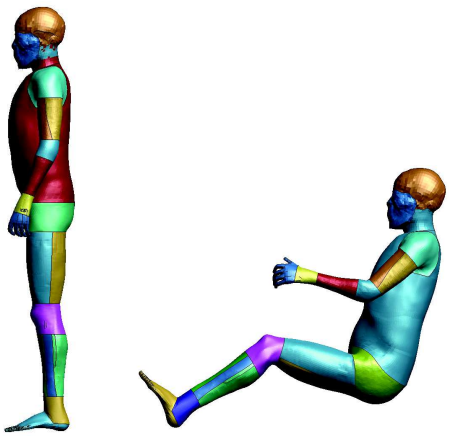

Figure 4.1 – Pedestrian and occupant versions of the THUMS model (THUMS Manual, Toyota Motor Corporation 2011)

The model has approximately 1300 parts, 1 800 000 elements and 630 000 nodes. Table 4.1 shows the different anatomical regions of the model along with the number of parts of those regions.

The abdomen of the model can be seen on Figures 4.2a and 4.2b. The properties of the main parts such as type and number of elements, density and material law are detailed in Table 4.2. Each volumetric part is coated by a shell part for contact purposes or to represent the capsule of the organs if they have one. The hollow organs are modelled as compressible with a simplified hyperelastic material model (`MAT_057: LOW_DENSITY_FOAM`) whereas the solid organs are modelled as

1. Computed Tomography

number	body region	number of parts
1	Lower Extremity - Right	129
2	Lower Extremity - Left	129
3	Abdomen and Pelvis	48
4	Internal Organs	60
5	Upper Extremity - Right	97
6	Upper Extremity - Left	97
7	Neck	156
8	Head	236
9	Thorax	321

Table 4.1 – Body regions of the THUMS pedestrian model (THUMS Manual, Toyota Motor Corporation 2011)

incompressible with a hyperelastic rubber material model (MAT_181: SIMPLIFIED_RUBBER), according to Shigeta et al. 2009. Those material models are detailed in Appendix C. The mechanical response of those models is based on an engineering stress / strain curve from uniaxial test data. The curves can be seen on Figures 4.2c and 4.2d. The liver data was obtained from Tamura et al. 2002 and the small and large intestine data was obtained from Yamada 1970.

part	type	number of elements*	material model	density ($kg\,m^{-3}$)	mass (kg)
thoracic fat	volumetric	43000	hyperelastic incompressible (MAT_181)	1100	0.985
abdominal fat	volumetric	84000	hyperelastic incompressible (MAT_181)	1100	2.276
liver	volumetric	59000	hyperelastic incompressible (MAT_181)	100	0.179
liver coat	shell	6500	orthotropic membrane (MAT_034)	900	0.147
pancreas	volumetric	1500	hyperelastic incompressible (MAT_181)	100	0.00291
pancreas coat	shell	600	orthotropic membrane (MAT_034)	900	0.0132
spleen	volumetric	1800	hyperelastic incompressible (MAT_181)	100	0.0588
spleen coat	shell	2900	orthotropic membrane (MAT_034)	900	0.0744
right kidney	volumetric	6100	hyperelastic incompressible (MAT_181)	100	0.0186
left kidney		6300			0.0191
right kidney coat	shell	1200	orthotropic membrane (MAT_034)	900	0.0334
left kidney coat		1200			0.0339
stomach	volumetric	6100	hyperelastic incompressible (MAT_181)	100	0.0161
stomach coat	shell	1400	orthotropic membrane (MAT_034)	900	0.0335
small intestine	volumetric	68000	hyperelastic compressible (MAT_057)	499	1.18
small intestine coat	shell	9600	orthotropic membrane (MAT_034)	1000	0.245
large intestine	volumetric	39000	hyperelastic compressible (MAT_057)	708	0.54
large intestine coat	shell	7000	orthotropic membrane (MAT_034)	1000	0.161
bladder	volumetric	4400	elastic fluid (MAT_001)	1000	0.118
bladder coat	shell	1500	orthotropic membrane (MAT_034)	1000	0.0314
left flesh	volumetric	42000	hyperelastic incompressible (MAT_181)	1100	7.09
right flesh					
left flesh coat	shell	8300	orthotropic membrane (MAT_034)	1000	0.248
right flesh coat					

Table 4.2 – Properties of the main parts of the THUMS abdomen
*Approximate number

Three main contacts are defined in the model. All the parts in the contact are checked for penetration with all the others. The skin contact (Figure 4.3a) contains 34 parts and represents the outer surface of the body. It prevents the regions of the model of penetrating the others. The body contact (Figure 4.3b) is made of 201 parts and manly includes bones connecting tissues. The organs contact (Figures 4.3c and 4.3d), made of 18 parts includes the shell parts covering the organs and shell parts surrounding the organs such as the pleura or the peritoneum parts. Contacts create a non-penetration condition between the parts they include. The other way to create non-penetration condition between parts used in the model is to have the parts sharing the same nodes at their interface. This technique is used to link together the different part sets mentioned above in the different contacts.

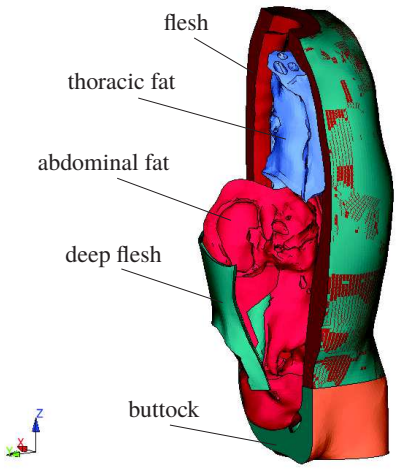

(a) Flesh and fat tissues

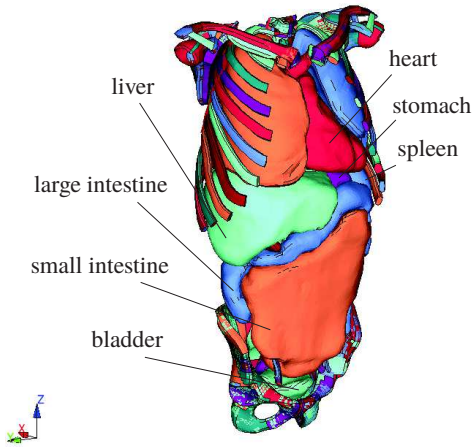

(b) Organs[a]

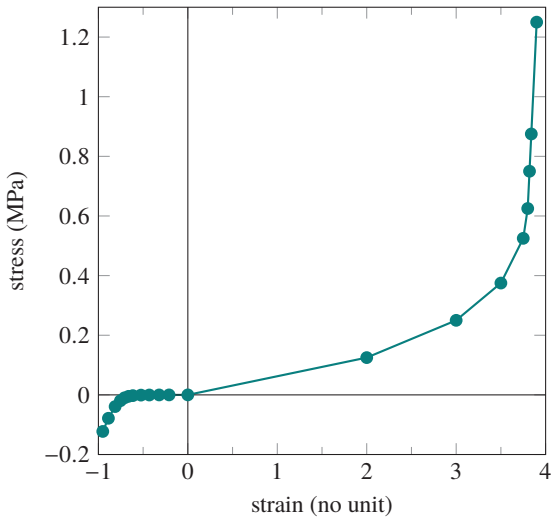

(c) Liver material curve[b]

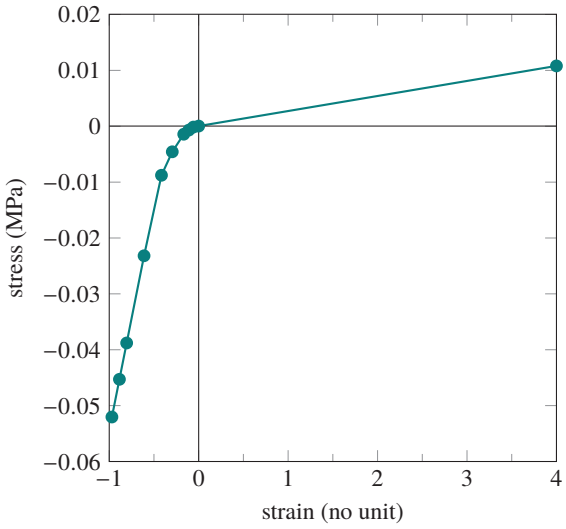

(d) Intestines material curve[b]

Figure 4.2 – Partial view and material curves of the main parts of the THUMS abdomen

[a]Flesh and fat parts have been hidden as well as pleurae, sternum, ribs cartilage and intercostal parts. Kidneys and pancreas can not be seen

[b]Positive and negative values represents the tension and compression characteristics, respectively

The simulations performed with the THUMS model were run using a fixed timestep of 4×10^{-4} ms achieved with mass scaling (as advised by Toyota Motor Corporation) and no gravity was applied.

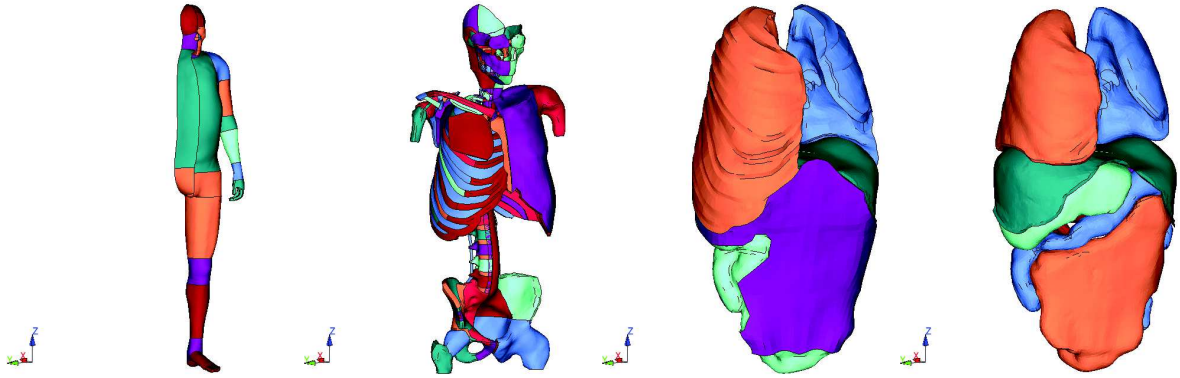

(a) Skin contact[a] (b) Body contact[a] (c) Organs contact (d) Organs contact (partial view)[b]

Figure 4.3 – Main contacts in the THUMS model (scale is not consistent across the pictures)
[a]Shell part on the right hand side of the model have been hidden for clarity
[b]Shell parts surrounding the organs have been hidden

4.2.2 Impactor simulations

Impactor tests from the literature were selected to be reproduced in simulation. Only results from Hardy et al. 2001 mid-abdomen 6 m s^{-1} will be presented here. Other configurations (Cavanaugh et al. 1986 and Hardy et al. 2001 upper abdomen) will not be presented. The model used was a model positioned for impactor test configuration by Toyota Motor Corporation, as used in Shigeta et al. 2009. The mass of the impactor was adjusted to 48 kg and its velocity was set to 6 m s^{-1}. The differences between the model and tests from Hardy et al. 2001 are the position of the legs, which are not straight and supported by the floor surface. The position of the arms is also different since in the model they are not hung to a hook above the subject. It has been chosen to keep the model that way, as no major influence on the response was forecasted.

To reproduce the mid-abdomen loading case from Hardy et al. 2001, the position of the impactor aligned with the L3 vertebra. The penetration was measured as the difference between y-coordinate of a node in the median plane of the impactor and a node on the back of the subject in line with the impactor node as seen on Figure 4.4b. The force is taken as the the y component of the contact force between the impactor as master part and the abdomen.

Figure 4.5c shows the simulation response in terms of force and penetration although slightly less penetration is predicted by the model. The response is in good agreement with the PMHS data from Hardy et al. 2001. However the response matchs better the test data when considering abdominal compression instead of penetration as shown on Figure 4.5d. The compression is the penetration of the impactor into the abdomen divided by the initial abdominal depth of the subject. This is to take into account the disparity between the abdominal depth of the THUMS model and those of the test subjects from Hardy et al. 2001 as shown on Table 4.3. The abdominal depth of the model is the difference between the y axis coordinates of the nodes shown on Figure 4.4b in the initial state of the simulation. Figure 4.6 shows the deformed shape of the model.

subject	gender	age (years)	stature (cm)	mass (kg)	abdomen depth (mm)
THUMS model	NA	NA	178	73	260
GI3	M	87	173	73	307
GI4	F	93	165	58	292
GI6	M	85	165	91	307

Table 4.3 – Abdominal depths of the THUMS model and subjects from Hardy et al. 2001

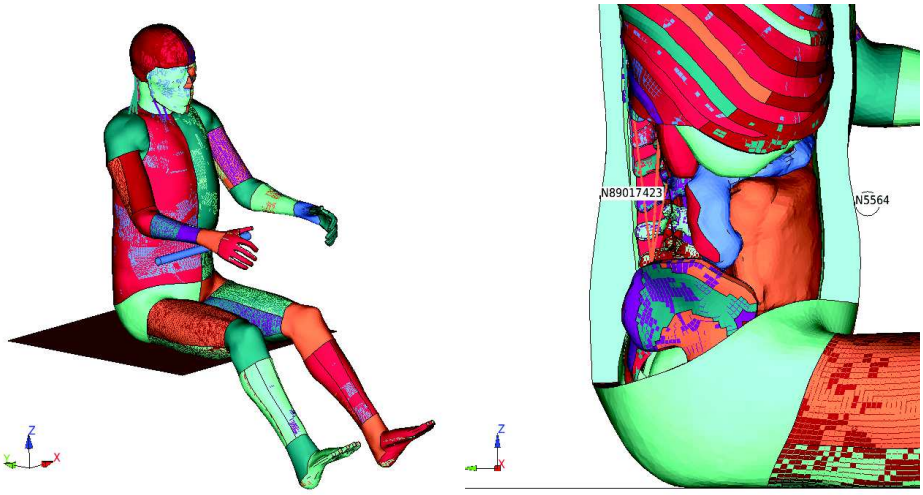

(a) Mid-abdomen impactor simulation

(b) Penetration measurement for impactor simulation

Figure 4.4 – Mid-abdomen impactor simulation setup and penetration measurement

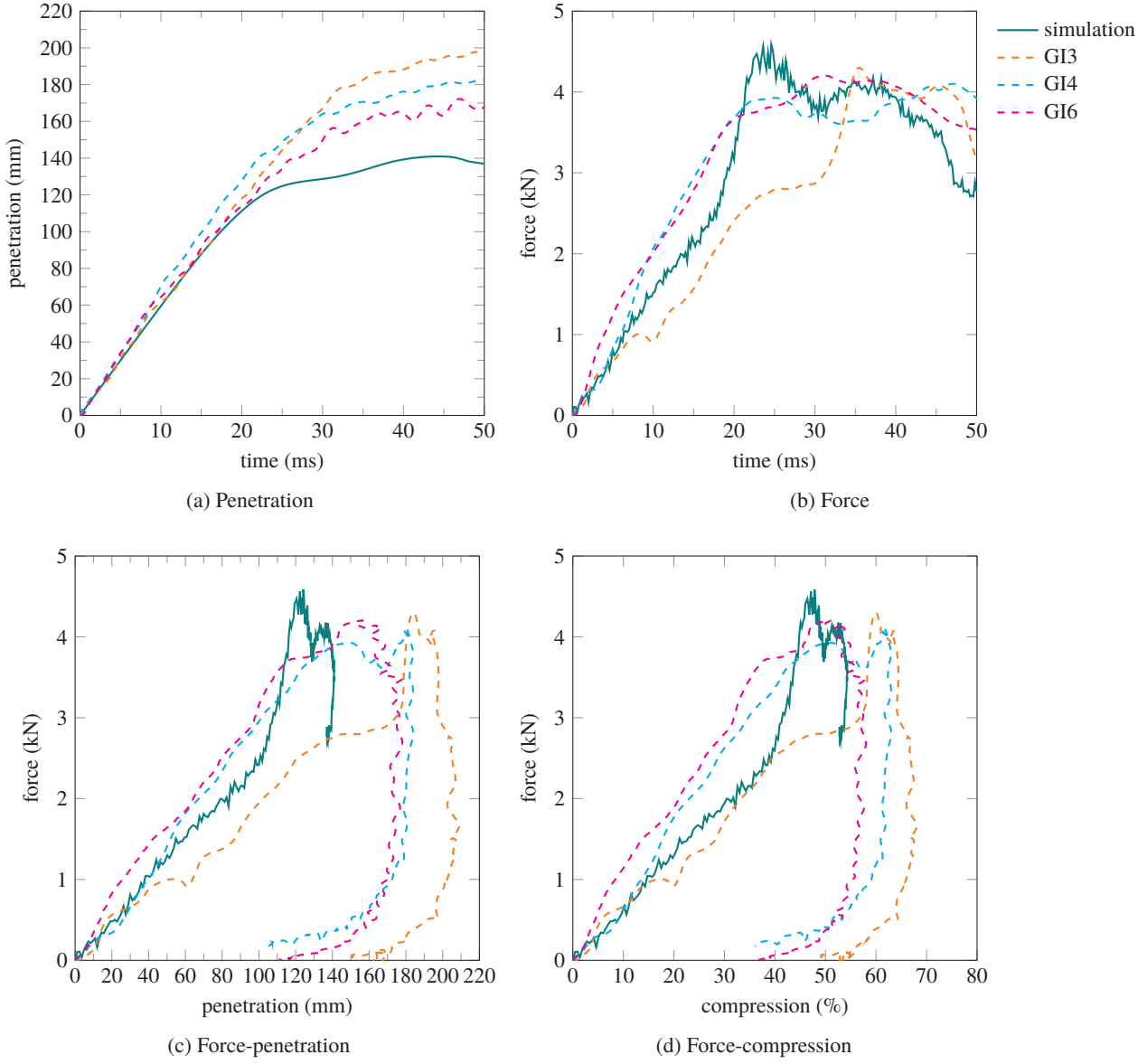

(a) Penetration

(b) Force

(c) Force-penetration

(d) Force-compression

Figure 4.5 – Mid-abdomen impactor 6 m s^{-1} simulation response versus PMHS from Hardy et al. 2001

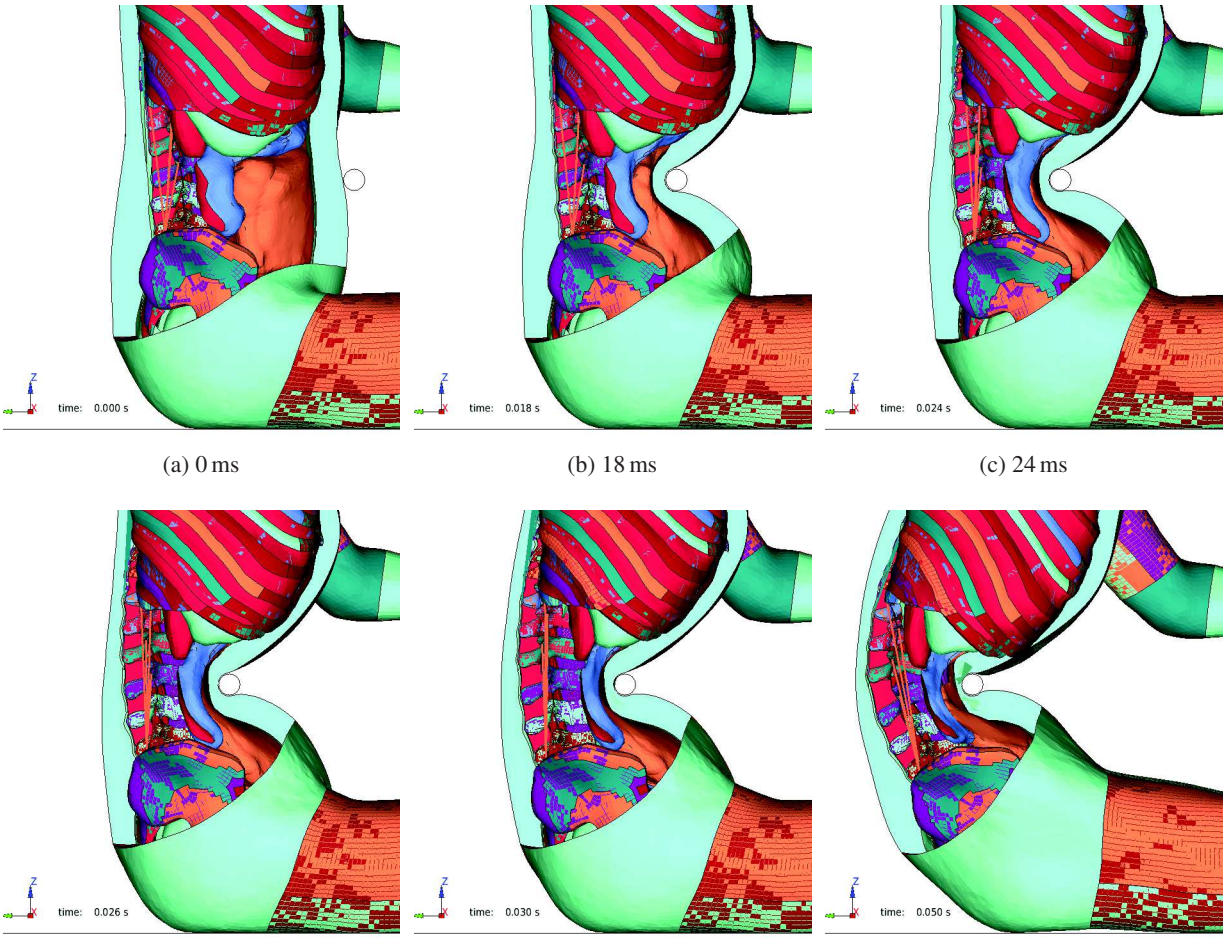

(a) 0 ms (b) 18 ms (c) 24 ms

(d) 26 ms (e) 30 ms (f) 50 ms

Figure 4.6 – Mid-abdomen impactor 6 m s^{-1} simulation deformed shape

4.2.3 Seatbelt simulations

Seatbelt tests from Foster et al. 2006 and Lamielle et al. 2008 were reproduced in simulation. Toyota Motor Corporation provided the model used in Shigeta et al. 2009. Due to chapter length considerations, only the two conditions from Lamielle et al. 2008 will be presented here.

4.2.3.1 Lamielle et al. 2008 MHA condition

For Lamielle et al. 2008 MHA tests the belt was pulled by an hydraulic jack with the objective of reaching a constant speed. Two target retraction velocities of $4\,\mathrm{m\,s^{-1}}$ (MHA111 and MHA151) and $5\,\mathrm{m\,s^{-1}}$ (MHA115 and MHA155) were used. Figure 4.7 shows the belt retraction, velocity and displacement profile of the MHA tests. Table 4.4 shows the characteristics of the PMHS subjects.

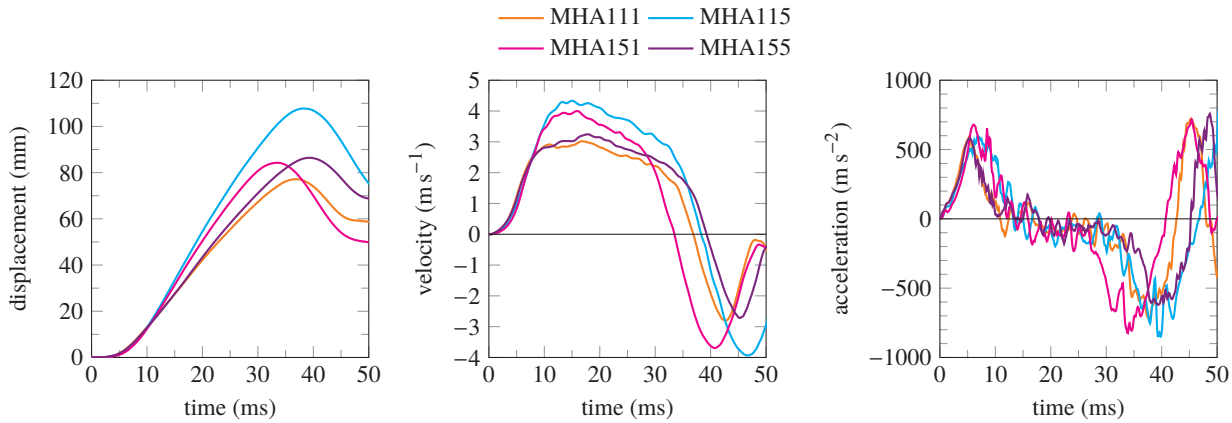

(a) Seatbelt retraction (b) Velocity (c) Acceleration

Figure 4.7 – Input conditions from Lamielle et al. 2008 MHA series

subject	gender	age (years)	stature (cm)	mass (kg)	abdomen depth (mm)
THUMS model	NA	NA	178	73	252
MHA111	M	74	175	77	287
MHA115	M	82	180	78	268
MHA151	M	88	166	69	249
MHA155	M	88	169	60	234

Table 4.4 – Abdominal depths of the THUMS model and subjects from Lamielle et al. 2008 MHA condition

In order to reproduce the PMHS test condition, it has been chosen to impose the belt retraction profile over time. All tests from the MHA condition were simulated and the THUMS model showed a lower force level than the PMHS data. Therefore, the test with the highest retraction velocity of all, MHA115, will be used as reference since it gave the highest force level of all the simulated cases.

Figure 4.8 shows the response of the model along with the PMHS curves. Penetration is in good agreement with the PMHS data, which is expected. The force magnitude is lower than the test data but the shape exactly the same the test responses.

Figure 4.8d compares the force between the back of the subject and the test bench, for the test data as well as for the simulation. The back force predicted by the simulation is lower than the test data, in the same proportions as the abdomen force. An other difference is that the simulated back force is phase-shifted compared to the test data. That is the back force from the simulation starts rising approximately 15 ms after the force from PMHS tests. This could be explained by how the

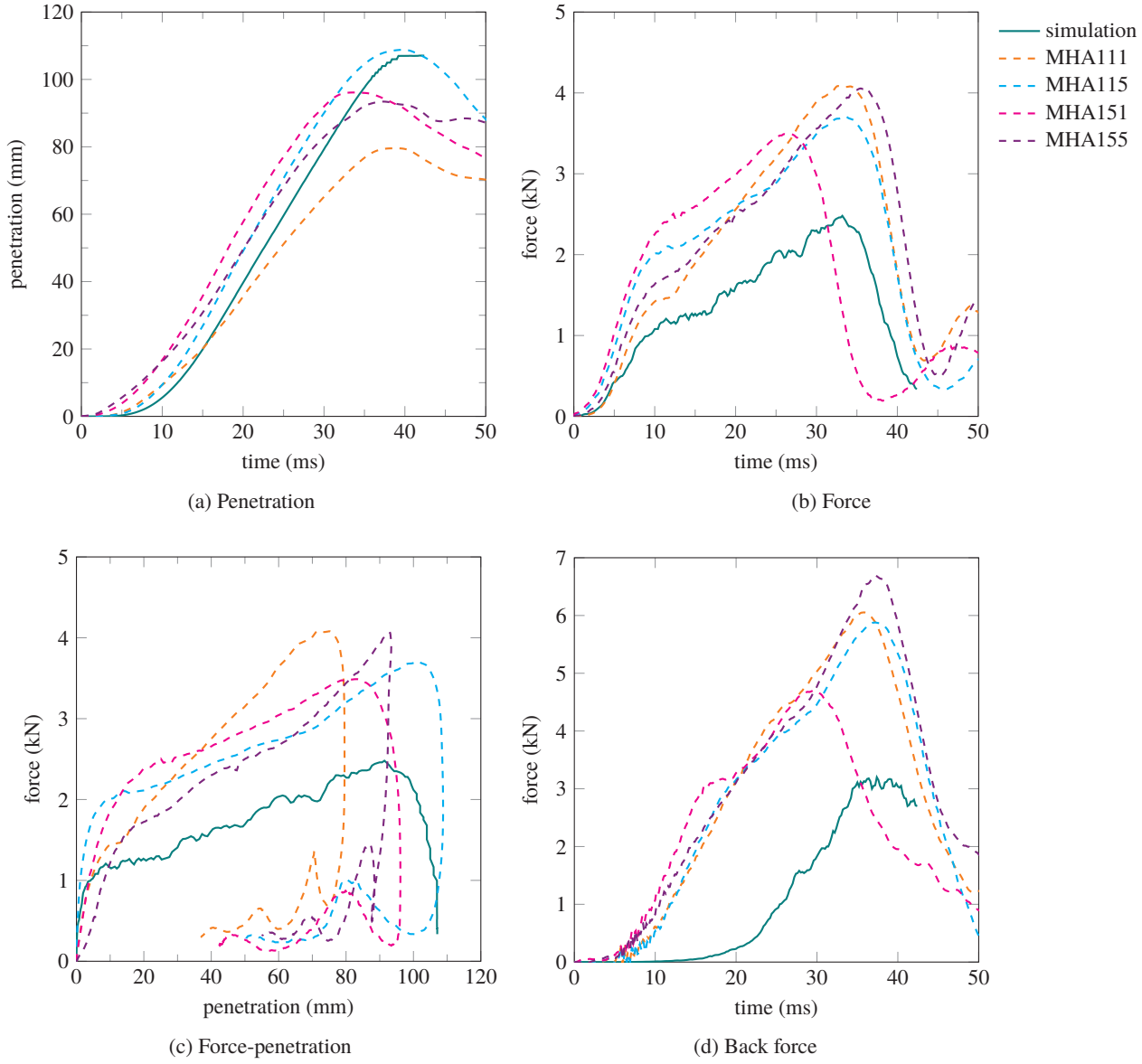

(a) Penetration

(b) Force

(c) Force-penetration

(d) Back force

Figure 4.8 – Simulation results of Lamielle et al. 2008 MHA115 condition

subject is positionned against the seatback in both cases. In the simulation, the model has been translated until its back became tangent to the seatback plane. The coupling between the subject and the seatback is therefore weak before the simulation starts. It is likely that in the PMHS set-up, the subject back is already deformed against the seatback before the test starts, therefore creating a stronger coupling.

Figure 4.9 compares the deformed shape of the simulation and images from the relevant PMHS test. In the PMHS test, the belt penetrates into the abdomen of the subject before the test starts. This initial penetration is due to the pre-tension of 20 N applied to the belt (10 N in each strand as mentioned in Lamielle et al. 2008). This applies to the PRT condition too where the initial penetration seems more important (see Figure 4.14d).

Figure 4.10 shows the deformation of the seatbelt during the simulation and Figure 4.11a superimposes the belt deformed shapes along the simulation with the umbilicus point as fixed reference point. According to Figure 4.11b, the peak of belt penetration into the abdomen is the same as the peak seatbelt retraction.

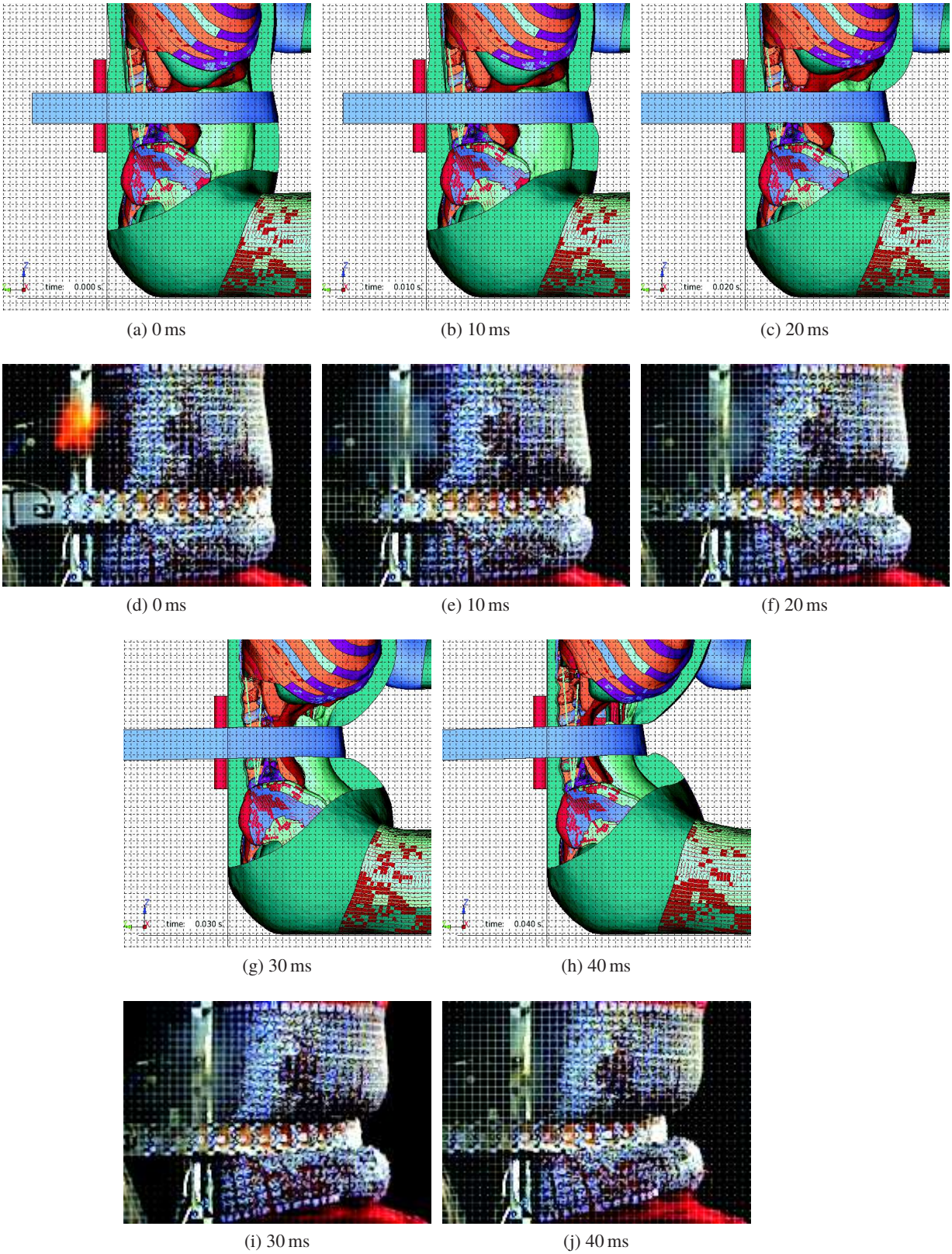

(a) 0 ms (b) 10 ms (c) 20 ms

(d) 0 ms (e) 10 ms (f) 20 ms

(g) 30 ms (h) 40 ms

(i) 30 ms (j) 40 ms

Figure 4.9 – MHA condition seatbelt simulation deformed shape compared with MHA115 PMHS images

The grid size is 10 mm

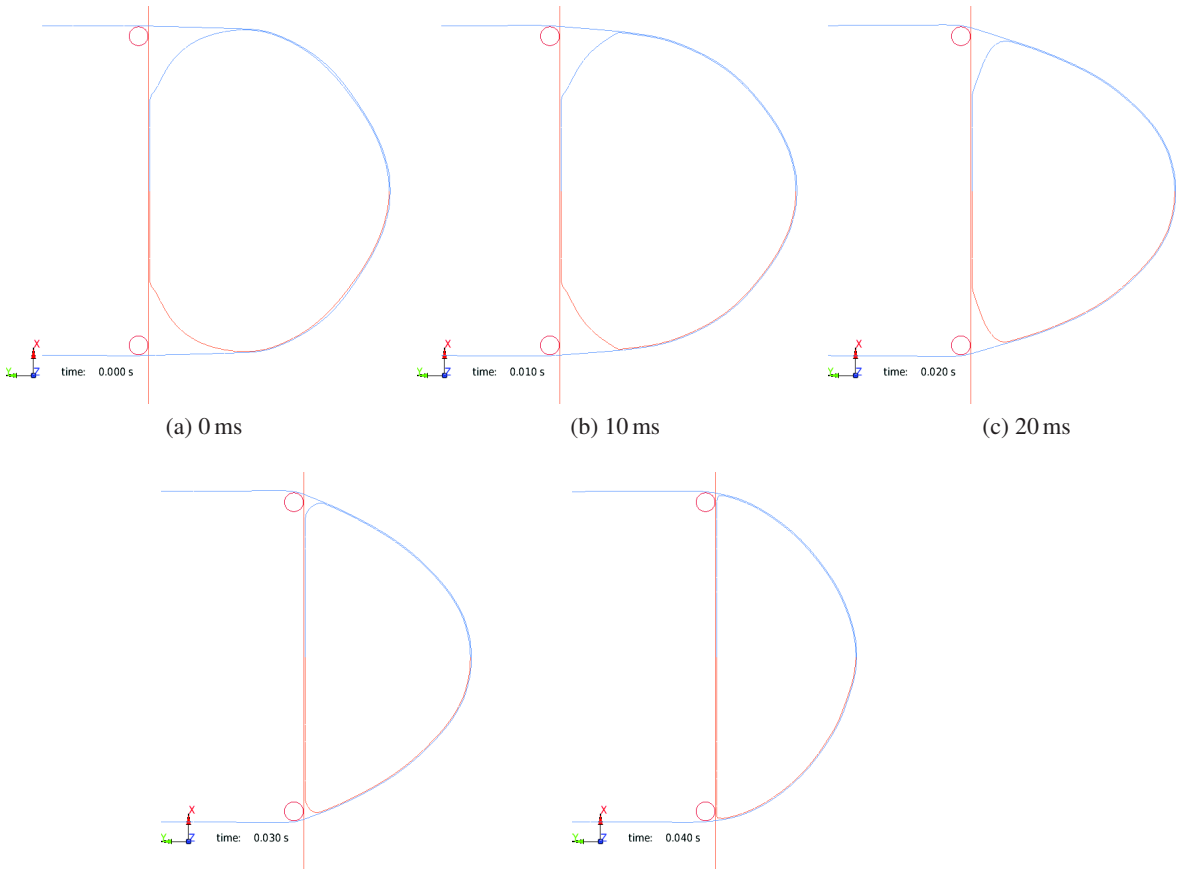

(a) 0 ms (b) 10 ms (c) 20 ms

(d) 30 ms (e) 40 ms

Figure 4.10 – Seatbelt deformation for MHA condition

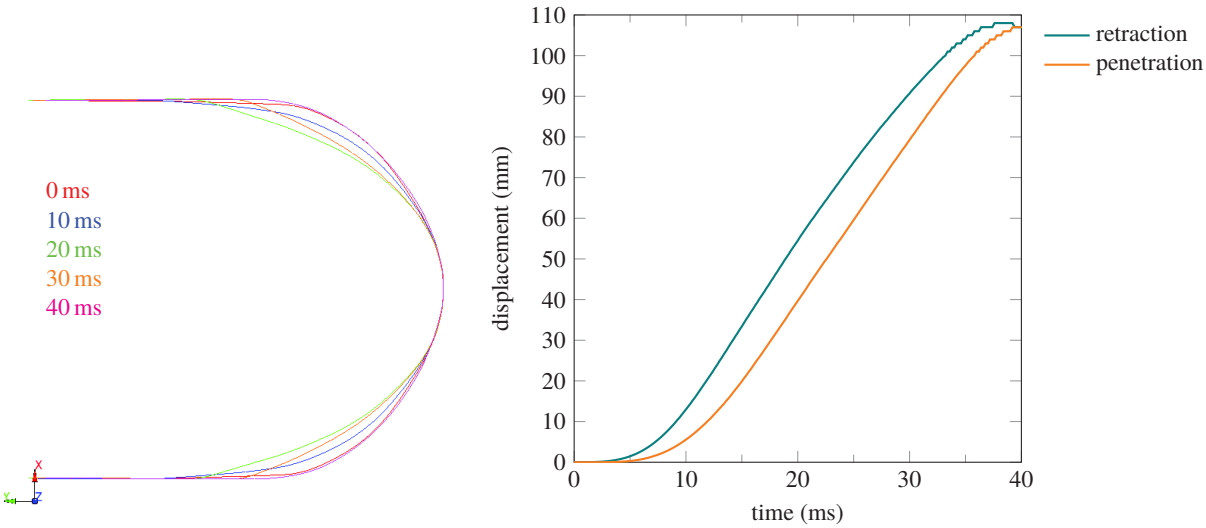

(a) Seatbelt deformation (b) Belt retraction and abdomen penetration

Figure 4.11 – Belt retraction and seatbelt deformation for MHA115 simulation

4.2.3.2 Lamielle et al. 2008 PRT condition

It has been chosen to impose the belt retraction profile over time from test data in order to simulate PMHS tests. All tests from the PRT condition were simulated. The THUMS model showed a lower penetration level than the PMHS data. Therefore, the test with the highest penetration of all, PRT052, will be presented here and used in this chapter since it results is the closest to PMHS data. Figure 4.12 shows the retraction conditions for the PRT tests and Table 4.4 shows the characteristics of the PMHS subjects.

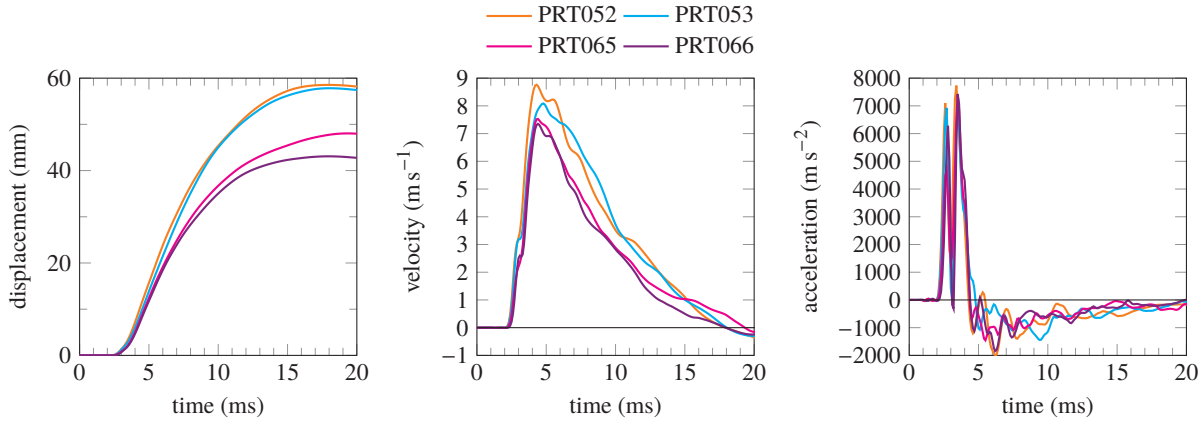

(a) Seatbelt retraction (b) Velocity (c) Acceleration

Figure 4.12 – Input conditions from Lamielle et al. 2008 PRT series

subject	gender	age (years)	stature (cm)	mass (kg)	abdomen depth (mm)
THUMS model	NA	NA	178	73	252
PRT052	M	72	162	54	222
PRT053	M	85	153	56	254
PRT065	M	88	172	72	243
PRT066	M	82	172	77	258

Table 4.5 – Abdominal depths of the THUMS model and subjects from Lamielle et al. 2008 PRT condition

As it can be seen on Figure 4.13a, the penetration response of the model goes lower than the test data after the initial loading phase. The peak belt retraction imposed in the simulation is 60 mm but the simulation gives a maximum abdomen penetration of 56 mm where 68 mm were expected. The interaction force between the belt and the abdomen (Figure 4.13b) has a magnitude comparable to test data but the profile over time of the force signal does not match the test data. The force in the simulation drops approximately 8 ms earlier compared to the PMHS results.

Regarding the back force comparison, the force magnitude in the simulation is much lower than in the test. A phase shift is observed in the back force, it can be explained the same way as for the MHA condition.

Figure 4.14 compares the deformed shape of the simulation and images from the relevant PMHS test. The fact that the model shows less penetration of the belt into the abdomen can be seen on the different pictures. It has been mentioned in Lamielle 2008 that for PRT tests (unlike the MHA tests), the belt retraction profile was different than the displacement of the umbilicus point of the abdomen. The umbilicus displacement was, after the initial period of the loading, higher than the belt retraction. This was believed to be the result of the lateral deformation of the abdomen causing more penetration of the belt into the abdomen compared to the belt retraction (the abdomen being incompressible). This also highlights the effect of the abdomen mass at higher velocities. However, this is not the case in our simulations. Figure 4.16b shows higher belt retraction than penetration all

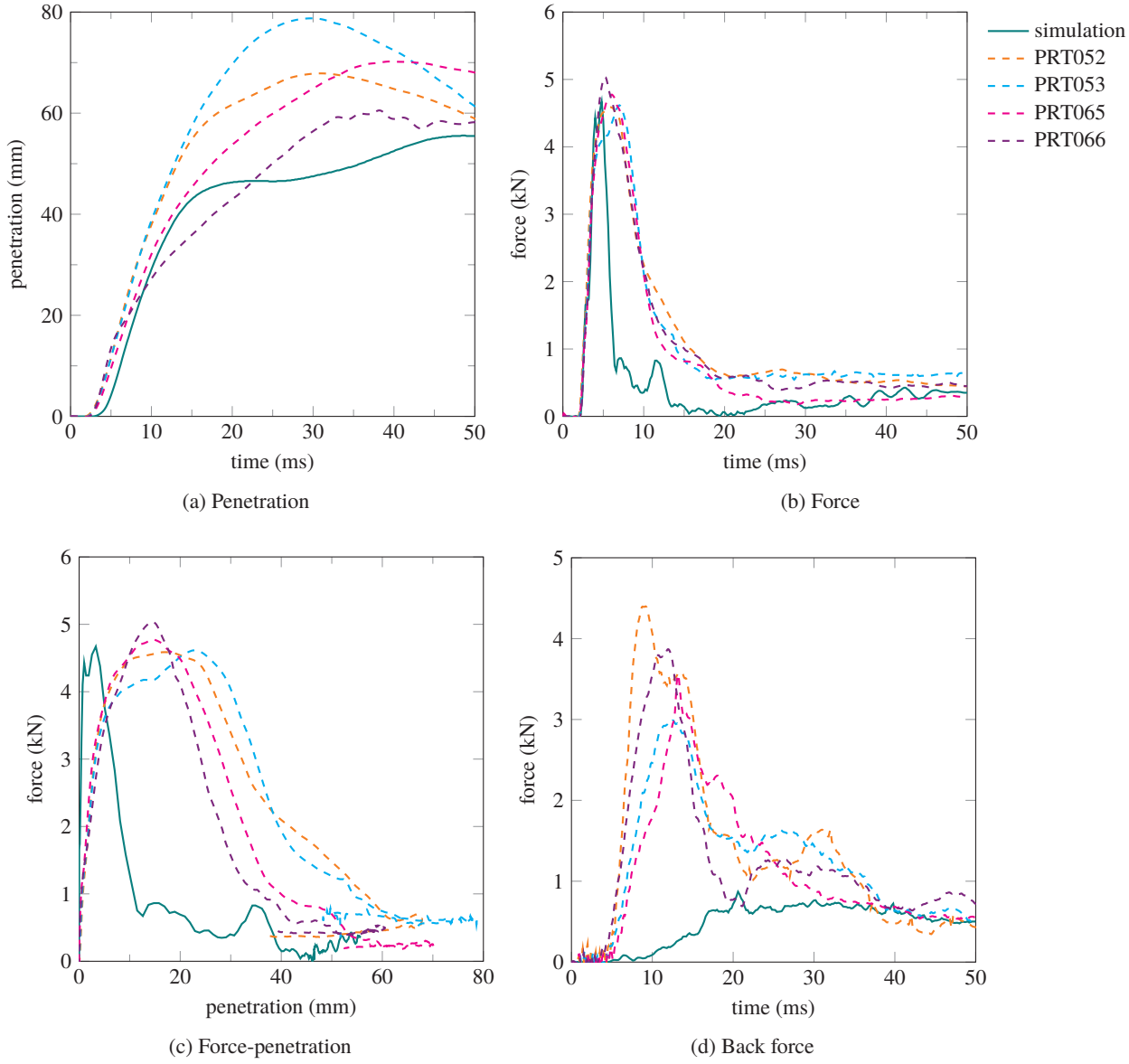

(a) Penetration

(b) Force

(c) Force-penetration

(d) Back force

Figure 4.13 – Simulation results of Lamielle et al. 2008 PRT052 condition

along the simulation, which could suggest that the mass effects that are observed in the PMHS data are not reproduced in the simulation. The incompressibility of the abdomen creates only very little lateral seatbelt deformation in the simulation (see Figures 4.15 and 4.16a).

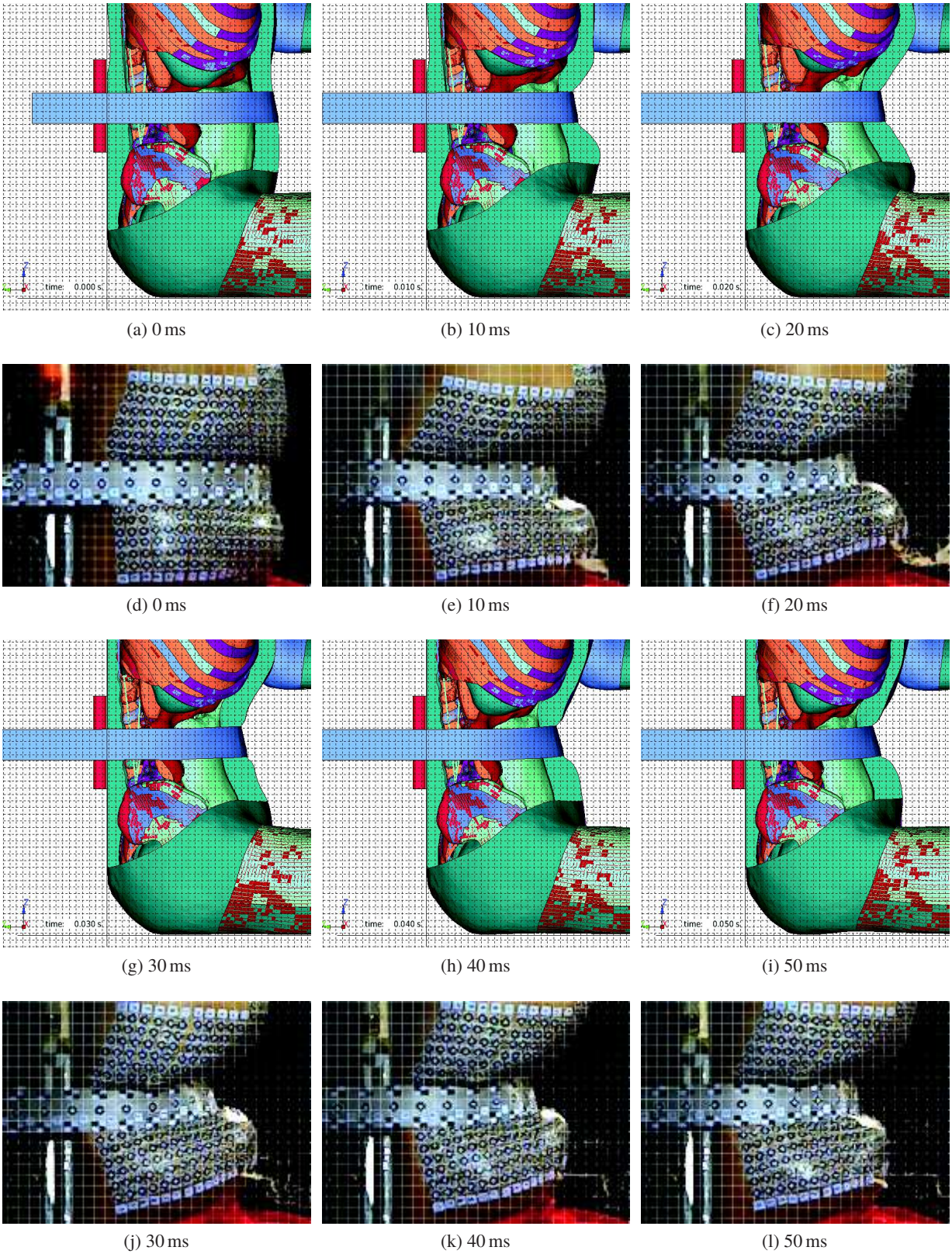

(a) 0 ms (b) 10 ms (c) 20 ms

(d) 0 ms (e) 10 ms (f) 20 ms

(g) 30 ms (h) 40 ms (i) 50 ms

(j) 30 ms (k) 40 ms (l) 50 ms

Figure 4.14 – PRT condition seatbelt simulation deformed shape compared with PRT052 PMHS images

The grid size is 10 mm

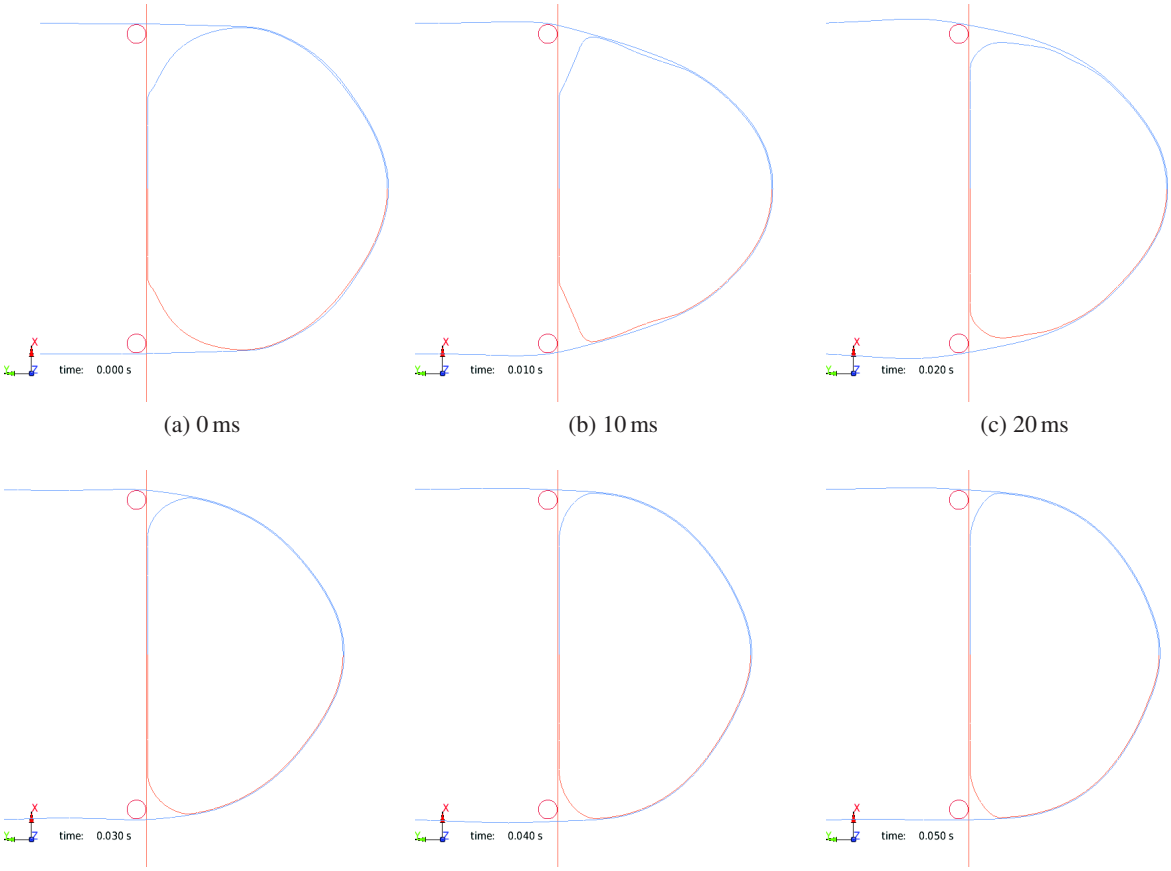

(a) 0 ms (b) 10 ms (c) 20 ms

(d) 30 ms (e) 40 ms (f) 50 ms

Figure 4.15 – Seatbelt deformation for PRT condition

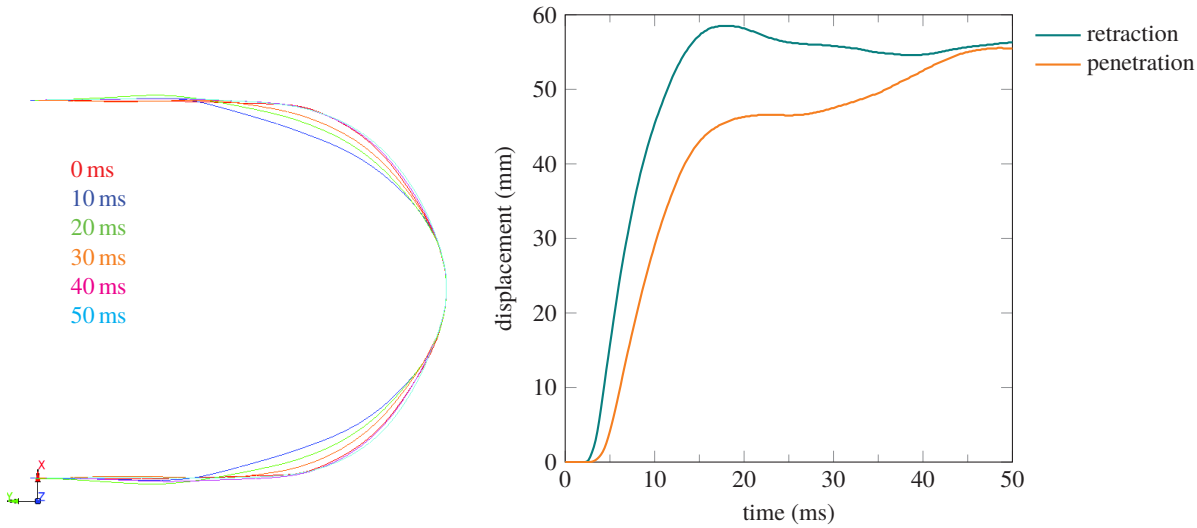

(a) Seatbelt deformation (b) Belt retraction and abdomen penetration

Figure 4.16 – Belt retraction and seatbelt deformation for PRT052 simulation

4.2.4 Conclusion on simulations with the THUMS model

Among the PMHS load cases reproduced with the THUMS model, only the impactor case from Hardy et al. 2001 at $6\,\mathrm{m\,s^{-1}}$ and the seatbelt cases from Lamielle et al. 2008 were presented here. The model response in terms of force and penetration is in good agreement with the tests data for most of the cases. For the MHA condition from Lamielle et al. 2008, the force level is however below the PMHS level probably due to the relatively low loading velocity for this condition compared to the other PMHS conditions. The rate-sensitivity of the THUMS model is therefore more adapted for highly dynamic loadings for which it had been initially validated in Shigeta et al. 2009.

Due to its detailed anatomical representation of the human body, the THUMS model could also be seen as a suitable tool for injury prediction under the confirmation that engineering parameter values extracted from the model are correlated to injury severity reported for the PMHS. This will be addressed in the following section.

4.3 Injury criteria using APTS pressure

It has been reported in Chapter 1, Section 1.2.4 that the only injurious study for impactor loading was Hardy et al. 2001 with liver injuries occurring in all the conditions. No injuries were reported in Cavanaugh et al. 1986, which is questionable given the fact that the impact velocities were similar to those of Hardy et al. 2001. Therefore, Cavanaugh et al. 1986 will not be considered for injury analysis.

Regarding seatbelt loading, Hardy et al. 2001 and Trosseille et al. 2002 did not report consistent injuries across all the subjects. Foster et al. 2006 reported liver injuries for the A condition and no injuries for the B condition. Lamielle et al. 2008 reported small intestine injuries for the MHA condition and small and large intestine injuries for the PRT condition. Mesentery injuries will be considered as small intestines injury since the mesentery is attached to the small intestine.

Given the scarcity of injury occurrence for a specific organ across all the different studies, all injuries reported in PMHS studies will be considered, which means injuries with AIS 2 or above. In practice, only the small intestine injuries from Lamielle et al. 2008 are AIS 2 injuries, all the other considered injuries are AIS 3 or above.

4.3.1 Internal energy as an injury measure for THUMS

Internal energy computed at the part level in the FE model has been chosen as an injury indicator for organs. The internal energy for a part is the sum of the internal energies of all the part's elements. Equation 4.1 defines the internal energy as mentioned in LS-DYNA Theory Manual (Hallquist 2006) for an element. Internal energy for an element is an incremental sum over time which includes the sum over the space direction of the product stress / incremental strain / volume. Therefore the internal energy represents both stress and strain states. Due to the important geometry variability between the PMHS subjects and the THUMS model, a global measure at the organ level is appropriate to estimate the injury risk to an organ.

$$e^{n+1} = e^n - \frac{1}{2} \cdot \triangle v \cdot \left(p^n + p^{n+1} + q^{n-\frac{1}{2}} + q^{n+\frac{1}{2}}\right) + v^{n+\frac{1}{2}} \cdot s_{ij}^{n+\frac{1}{2}} \cdot \triangle \varepsilon_{ij}^{n+\frac{1}{2}}$$

$$\text{With: } \begin{cases} e \text{ the element internal energy} \\ v \text{ the element volume} \\ q \text{ the bulk viscosity} \\ p \text{ the pressure} \\ s_{ij} \text{ the deviatoric stress components} \\ \varepsilon_{ij} \text{ the strain components} \\ n \text{ the timestep} \\ \triangle v = v^{n+1} - v^n \\ v^{n+\frac{1}{2}} = \frac{1}{2} \cdot \left(v^n + v^{n+1}\right) \end{cases} \tag{4.1}$$

4.3.2 Correlation between internal energy values from THUMS and PMHS injuries

In order to determine if engineering parameters from the THUMS model can be used for injury prediction, the maximum values of internal energy for each organ are compared to the injury outcome from PMHS studies on Figure 4.17. It stands out that the organs internal energy values are correlated with the injury outcome only for the liver. The small and large intestine present a negative correlation between injuries and internal energy. However, the liver is the organ with the lowest energy values among the three injured organs. This is explained by the fact by the liver is not

directly loaded by the seatbelt or the impactor at the mid-abdomen level in the model. However, in a PMHS test the liver position can vary due to anthropometric differences and it is likely that the abdominal organs shift in the inferior direction when considering PMHS compared to healthy subject due to the post-mortem lack of muscles tension. Howes et al. 2013 reported that markers placed on the liver of a post-mortem subject had a displacement of between 55 mm and 111 mm in the superior direction when the subject was placed from head up to head down. This explains why liver injuries are seen in PMHS studies while the loading parameters of the FE model have relatively low values. The injury observed to the liver in PMHS tests could also be due to an indirect loadings such as pressure increase in the liver due to the loading of an other region of the abdomen.

The fact that no correlation appear for injuries to the small and large intestine is due to the fact that such injuries were only observed in one study, Lamielle et al. 2008. This study is the only considered study to have perfused the PMHS subjects at the organ level in addition to the arteries (see Table B.3 in Appendix), therefore allowing to see contusions in those organs. Furthermore, Howes et al. 2015 reported that in order to detect jejunum injuries, the presence of fluid or air in the loaded portion of the organ was necessary. There could therefore have been a variety of different conditions in the literature studies which did not lead to detect injuries.

The evaluation of injury measures based on the THOR APTS pressures measurements will be undertaken based on the liver data only.

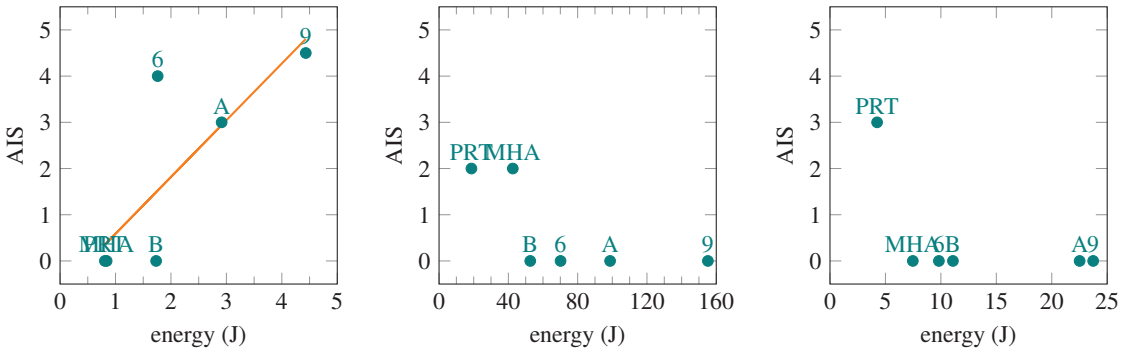

(a) Liver (b) Small intestine (c) Large intestine

Figure 4.17 – THUMS internal energies maximum values and AIS values
6: Hardy et al. 2001 6 m s^{-1} condition
9: Hardy et al. 2001 9 m s^{-1} condition
A: Foster et al. 2006 A condition
B: Foster et al. 2006 B condition
MHA: Lamielle et al. 2008 MHA condition
PRT: Lamielle et al. 2008 PRT condition

4.3.3 Selection of an injury measure based on pressure values from THOR

In order to assess if the pressure measurements from the THOR APTS sensors are representative of a particular organ injury mechanism or if it can be used as a global injury indicator, the pressure values will be compared to the internal organ energy from THUMS simulations. Due to the symmetrical nature of the different loadings, it has been chosen to average the left and right APTS pressures for a given loading case. The internal energy of the liver, small intestine and large intestine was extracted from the simulation results for each condition.

The improved prototype dummy abdomen described in Chapter 3, with the unified foam blocks have been used for APTS pressure assessment.

Figures 4.18 and 4.19 compare the APTS pressures from THOR simulations with the organs internal energy from THUMS simulations for impactor and seatbelt loading cases. What stands out is that

internal energies of the organs are always ranked in the same way. This means that the organs internal energies in the THUMS represent well the loading severity. Indeed, for seatbelt case, the internal energy ranking follows the ranking of maximum penetration velocity of the seatbelt in the abdomen or maximum abdomen compression (see Table B.2, in Appendix). In order of severity, the conditions are: Foster et al. 2006 A and B, Lamielle et al. 2008 PRT. However, Lamielle et al. 2008 MHA condition has the lowest penetration velocity values but shows higher internal energies than the PRT condition. This is due to the fact the MHA condition is the only non-pretensioner condition, having a slower velocity increase and higher abdomen compression than the PRT condition. The pressure measurement from the APTS follows the same ranking, although with close value for the two Foster et al. 2006 condition and Lamielle et al. 2008 MHA condition, with the presence of a phase shift.

Candidate injury measures based on pressure measurements have been computed from THOR simulations. The considered measures are $P_{\max}$, $\dot{P}_{\max}$ (both reported in Kremer et al. 2011 and Beillas et al. 2012) and $\dot{P}_{\max} \cdot P_{\max}$ (reported in Johannsen et al. 2007 and Beillas et al. 2012). The value of those measures are reported in Table 4.6 and Figure 4.20 shows the correlation between the injury measures and organ internal energies from THUMS simulations for the liver only, following the conclusions from the previous section. A linear regression has been performed for each data series. The measure best correlated with the energy levels is $\dot{P}_{\max} \cdot P_{\max}$ with a R^2 value of 0.44, followed by the $P_{\max}$ measure. The measure $\dot{P}_{\max}$ does not correlate with the energy levels, the R^2 value being of 0.14 and the p-value of 0.47. The measures that correlate with the internal energies from the THUMS model for each of the three injured organs are judged suitable to investigate the link between their values and the injury outcome.

condition	measure			internal energy		
	$P_{\max}$ (bar)	$\dot{P}_{\max}$ (bar s^{-1})	$\dot{P}_{\max} \cdot P_{\max}$ (bar^2 s^{-1})	liver (J)	small intestine (J)	large intestine (J)
A	1.5	299	448	2.9	99	23
B	1.1	153	176	1.7	53	11
MHA	1.3	47	61	0.8	43	7
PRT	0.7	181	131	0.8	19	4
6	2.1	103	216	1.8	70	10
9	1.9	146	273	4.4	155	24

Table 4.6 – Injury measures and internal energy peak values
6: Hardy et al. 2001 6 m s^{-1} condition
9: Hardy et al. 2001 9 m s^{-1} condition
A: Foster et al. 2006 A condition
B: Foster et al. 2006 B condition
MHA: Lamielle et al. 2008 MHA condition
PRT: Lamielle et al. 2008 PRT condition

This page was intentionally left blank.

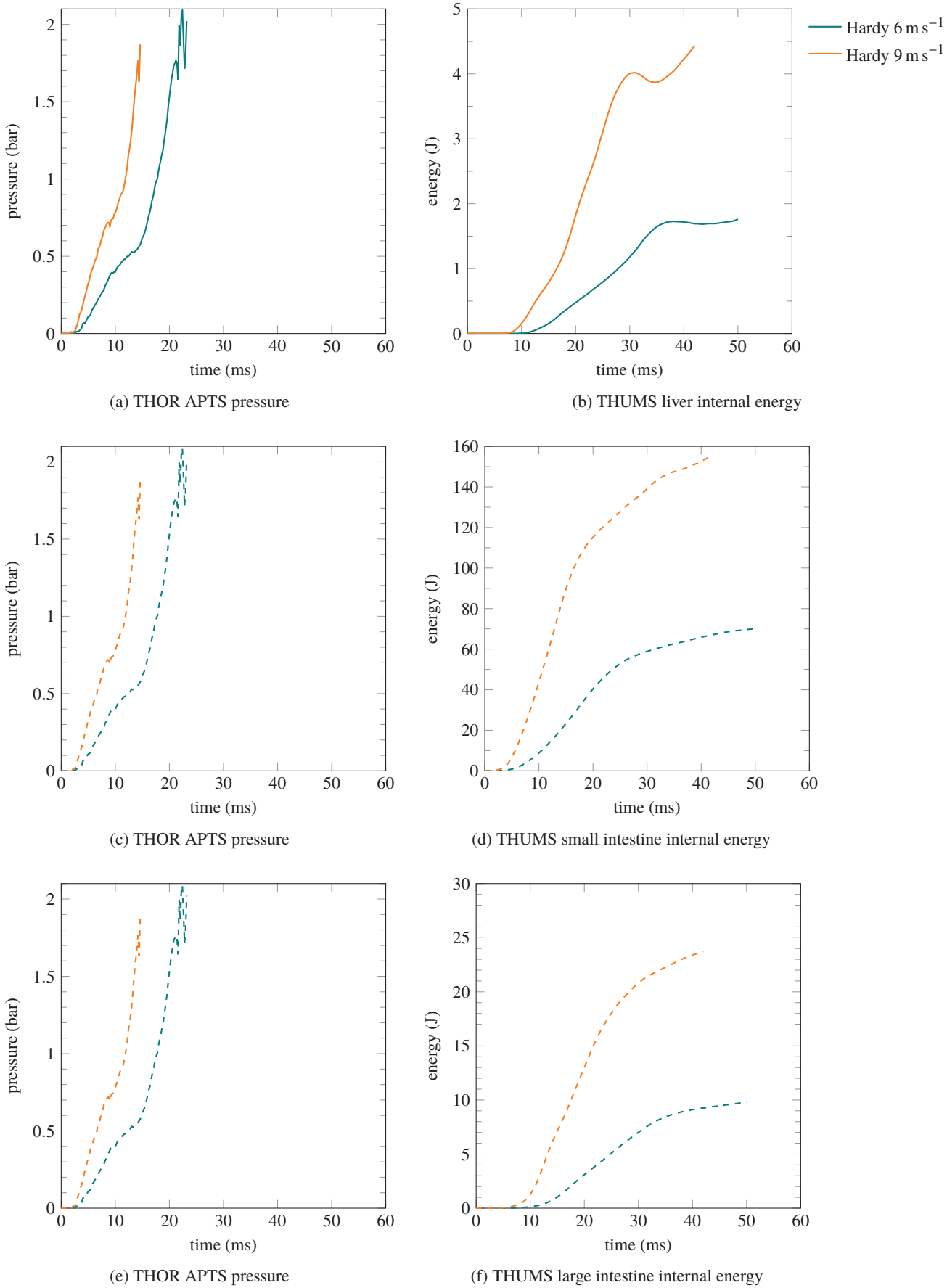

(a) THOR APTS pressure

(b) THUMS liver internal energy

(c) THOR APTS pressure

(d) THUMS small intestine internal energy

(e) THOR APTS pressure

(f) THUMS large intestine internal energy

Figure 4.18 – THOR APTS pressure and THUMS internal energies for impactor case
Solid lines: injurious loading
Dashed lines: non injurious loading

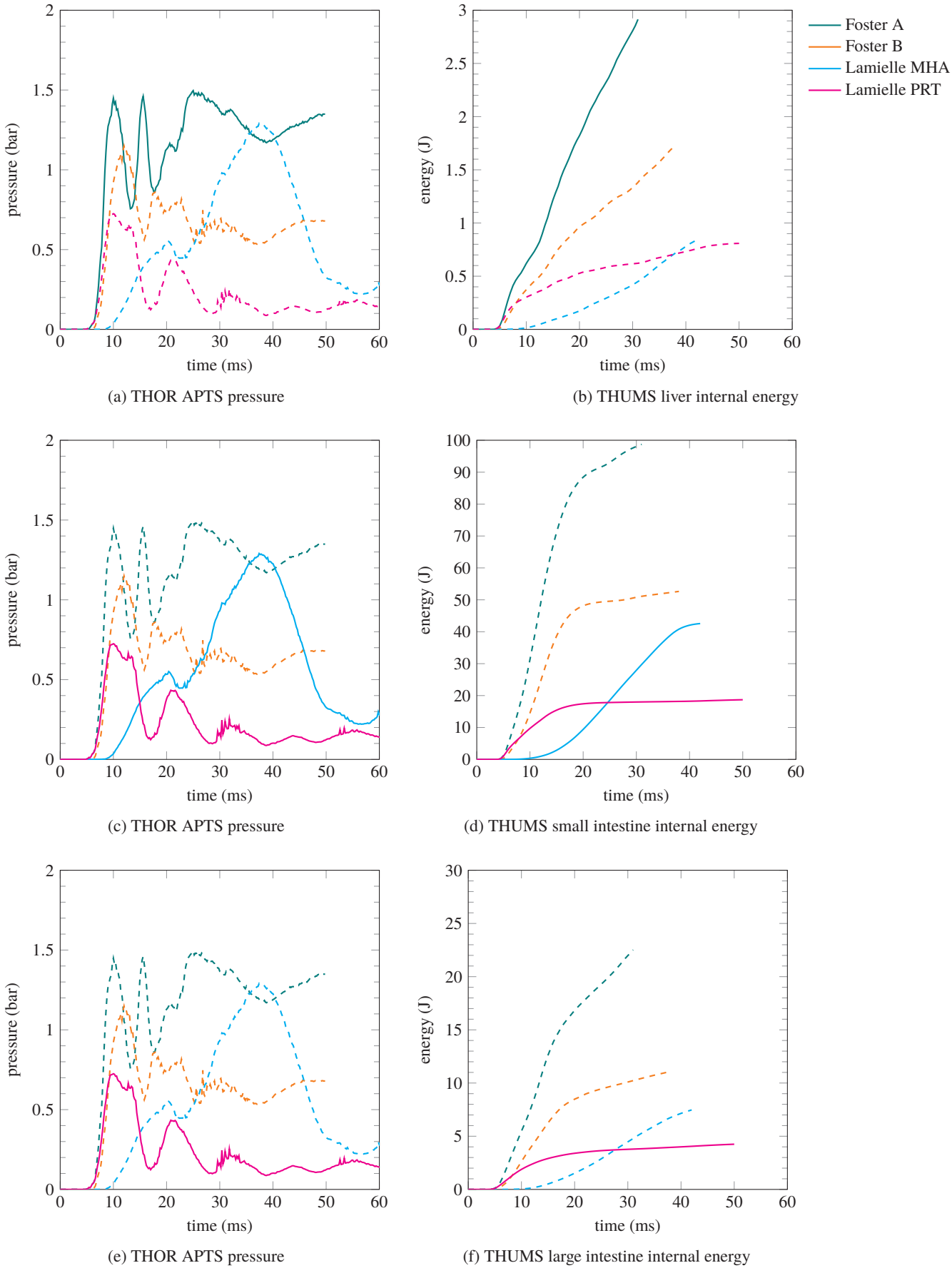

(a) THOR APTS pressure

(b) THUMS liver internal energy

(c) THOR APTS pressure

(d) THUMS small intestine internal energy

(e) THOR APTS pressure

(f) THUMS large intestine internal energy

Figure 4.19 – THOR APTS pressure and THUMS internal energies for seatbelt case
Solid lines: injurious loading
Dashed lines: non injurious loading

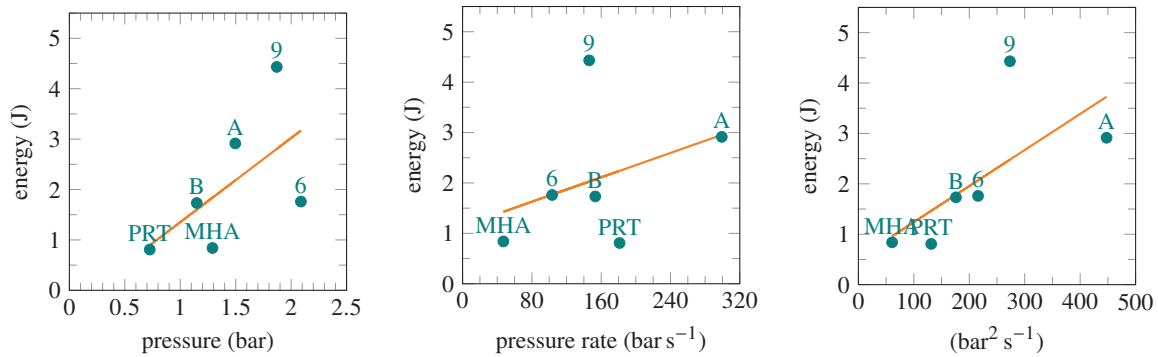

(a) P_{max}
$R^2 = 0.36$
p-value: 0.21

(b) $\dot{P}_{max}$
$R^2 = 0.14$
p-value: 0.47

(c) $\dot{P}_{max} \cdot P_{max}$
$R^2 = 0.48$
p-value: 0.13

Figure 4.20 – THOR injury measures and THUMS internal energies maximum values for the liver
6: Hardy et al. 2001 6 m s^{-1} condition
9: Hardy et al. 2001 9 m s^{-1} condition
A: Foster et al. 2006 A condition
B: Foster et al. 2006 B condition
MHA: Lamielle et al. 2008 MHA condition
PRT: Lamielle et al. 2008 PRT condition

4.3.4 Injury criteria based on pressure

The selected injury measures based on the pressure measured by the APTS are P_{max} and $\dot{P}_{max} \cdot P_{max}$. Figure 4.21 presents the injury AIS 3+ values plotted versus the candidate measures values for the liver. Only the liver injury values present a profile that can be fitted by an injury risk curve, due to the lack of correlation between injuries and other parameters for the intestines as explained earlier. A Weibull distribution was used with a survival model as desbribed in Kent et al. 2008. The distribution states that the probability of injury $p(I)$ is linked to the the probability of "surviving" $p(S)$ by the relation $p(I) = 1 - p(S)$. The Weibull distribution uses a scale (η) and a shape factor (φ) in order to express $p(S)$ as in Equation 4.2 where x is the injury criterion. A Scilab program using the `optim` function was used to fit the Weibull function by adjusting the parameters η and φ. Table 4.7 shows the values of the scale and shape factor for the generated distributions along with the 50 % injury threshold, the x value so that $p(I) = 0.5$. In this case, the threshold values are very close to the scale factor values since the criteria values do not overlap for the injurious and non injurious conditions which gives a neat distinction by the Weibull function. Criteria values of $P_{max} = 1.46$ bar and $\dot{P}_{max} \cdot P_{max} = 209$ bar^2 s^{-1} represent a 50 % injury threshold.

$$p(S) = e^{-\left(\frac{x}{\eta}\right)^{\varphi}} \tag{4.2}$$

criterion	η	φ (no unit)	50 % injury threshold
P_{max}	1.46 bar	170	1.46 bar
$\dot{P}_{max} \cdot P_{max}$	209 bar^2 s^{-1}	120	209 bar^2 s^{-1}

Table 4.7 – Injury criteria values for AIS 3+ liver injuries

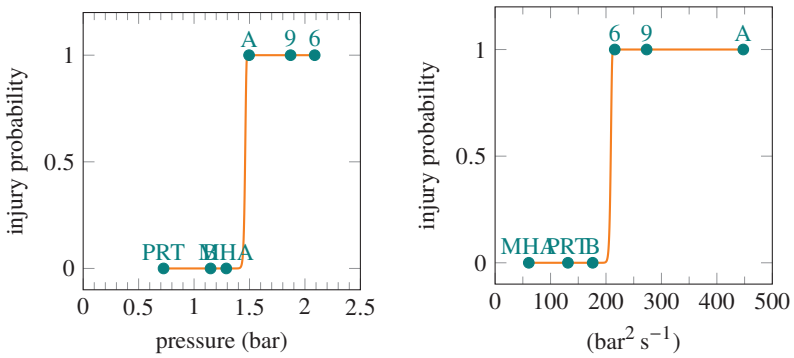

(a) P_{max} (b) $\dot{P}_{max} \cdot P_{max}$

Figure 4.21 – Candidate injury criteria for the liver
6: Hardy et al. 2001 6 m s^{-1} condition
9: Hardy et al. 2001 9 m s^{-1} condition
A: Foster et al. 2006 A condition
B: Foster et al. 2006 B condition
MHA: Lamielle et al. 2008 MHA condition
PRT: Lamielle et al. 2008 PRT condition

4.3.5 Conclusion on injury criteria

Organs internal energy from THUMS simulations have been used to assess the relevance of pressure injury measures. The only organ for which pressure measures lead to a link with injuries is the liver. No injury criteria could be defined for the small and large intestines due to the fact that injuries were not ranked in the same order as the considered injury measures. For the liver, the injury measure $\dot{P}_{max}$ was rejected due to lack of correlation with the organ internal energy from THUMS. The most significant injury measure was $\dot{P}_{max} \cdot P_{max}$ followed by P_{max}.

The distinction between the liver and the small and large intestines is that the liver is a solid organ and the intestines are hollow organs. In this study the attempt was made to find a single injury criterion for all types of organs, in order to have a reliable criterion to use with the dummy abdomen measurements. But since the nature of the organs are different, different injury criteria could be considered for both types of organs if more injurious data for hollow organs were available. The fact that only six loading conditions from the literature presented consistent injury statements across a majority of subjects also reduces the statistical strength of the injury criteria.

4.4 Conclusion

The validation of the THUMS model has been assessed for a wide range of loading conditions (six in total). The internal energy of the THUMS organs was extracted in order to assess the loading severity of each organ (liver, small intestine, large intestine) injured in PMHS tests from the literature. The correlation between energy and injuries was successful for the liver only. Candidate pressure measures with the THOR prototype abdomen have been selected for injury prediction for the liver based on the correlation with injury levels. The measures $P_{\max}$ and $\dot{P}_{\max} \cdot P_{\max}$ have then been linked to the the injuries from PMHS studies and criteria could be defined for the liver. $P_{\max} = 1.46\,\text{bar}$ and $\dot{P}_{\max} \cdot P_{\max} = 209\,\text{bar}^2\,\text{s}^{-1}$ represent a 50 % liver injury risk. No criteria could be defined for the other injured organs in PMHS studies, the small intestine and the large intestine. This is due to difficulties in assessing injuries for those organs in PMHS tests. The fact that the proposed injury criteria are based on only six conditions (three injurious and three non-injurious) is a limit of the statistical significance of the criteria.

Conclusion

A first objective of this work was to improve the biofidelity of the THOR dummy prototype abdomen developed by IFSTTAR and Toyota Motor Europe. This has been done by unifying the front foam blocks and a material change for the abdomen has been considered. A second objective was to develop a specific injury criterion based on the APTS sensors pressure measurements. A first step has been to asses the influence of the dummy torso flexion on the APTS reading during sled tests. In a second step, using local engineering parameters from the THUMS model at the organ level allowed to select suitable injury measures based on pressure and to link them with organ injuries from PMHS tests.

Chapter 1 showed that there is a global need to decrease the number of road fatalities, frontal impact being the most common crash case. The abdomen is a crucial region regarding serious to critical injuries, especially for rear passengers and in case of submarining. However, no injury criterion for the abdomen is applied currently. The biofidelity of the THOR dummy abdomen needs to be improved and its sensors measurement needs to be linked to an injury risk. The recent abdomen prototype developed by IFSTTAR and Toyota has shown better biofidelity than the standard abdomen and is equipped with APTS sensors that are candidates for providing pressures measurements for injury prediction. Recently developed finite element models of the human body having a highly detailed geometry of the abdominal organs could also help for injury prediction based on engineering parameters obtained from impact simulations.

In Chapter 2, the finite element model of the THOR dummy has been improved in order to have a model response correlating better with the test data. Based on these improvements, the abdomen prototype finite element model has been included in the dummy finite element model. This new model allows to reproduce the prototype abdomen response under seatbelt and impactor test.

Chapter 3 presented the use of a lumped element model which showed that the THOR dummy abdomen was more elastically and less viscously deformable than the human abdomen. Material and design changes of the abdomen that would allow a more biofidelic response were implemented in the FE model of the prototype abdomen. The unification of the two foam layers of the abdomen improved the biofidelity. A material change for the unified foam block toward a visco-elastic material with an increased viscous contribution proved to be able to improve the biofidelity for some loading conditions. However, the prototype abdomen influences the dummy behaviour in sled tests, showing more hip point displacement and more pelvis rotation. The interaction force between the upper and lower abdomen is also increased by the prototype abdomen presence but no biofidelity reference exist for this phenomenon. Only static spine stiffness assessments have been performed in Luet et al. 2012 which does not provide information on the abdomen behaviour during such loading. Further design changes would be needed to overcome these issues and have a really biofidelic submarining behaviour.

The validation of the THUMS model has been assessed in Chapter 4 for a wide range of loading conditions (six in total). The internal energy of the THUMS organs was extracted in order to assess the loading severity of each organ (liver, small intestine, large intestine) injured in PMHS tests from the literature. Based on these internal energy values, candidate pressure measures from the THOR prototype abdomen have been selected for injury prediction. The measures $P_{\max}$ and $\dot{P}_{\max} \cdot P_{\max}$ have then been linked to the the injuries from PMHS studies and a criterion could be defined for the

liver. $P_{max} = 1.46\,bar$ and $\dot{P}_{max} \cdot P_{max} = 209\,bar^2\,s^{-1}$ represent a 50 % liver AIS 3+ injury risk. No criteria could be defined for the other injured organs in PMHS studies, the small intestine and the large intestine. This is due to difficulties in assessing injuries for those organs in PMHS tests.

The findings of this work being mainly based on simulation results, this implies limitations. The THOR finite element model abdomen validation has been improved during this work by implementation of more detailed material characteristics. However the validation of the model in sled tests is limited regarding pelvis rotation and lap belt forces which raises the question on the correct reproduction of the physical dummy submarining phenomenon.

Other limitations of this work is the fact that all conclusions based on PMHS results do not represent a healthy car passenger. The lack of muscle tension may modify the mechanical response under impact. This lack of tension will also affect the position of the organs in the body, the organs having a tendency to go down in the abdominal cavity without tension, resulting in a larger abdomen depth for PMHS compared to healthy subjects. Therefore the use of a finite element model of the human body such as THUMS with an average healthy male geometry to reproduce PMHS tests is not an exact reproduction of the test. The use of PMHS subject also questions the validity of injury statements, since the organs are not in their physiological state and that there is a dependency on the perfusion method.

More generally, the use of crash test dummies is also not perfectly representative of the real behaviour of car occupants during a crash. Dummies being a passive device, their pre-crash position is not representative of an active human occupant. It seems that this limit will always be inherent to dummies. Therefore, the development of active human body models representative of the human passenger reactions would allow to perform virtual crash tests in the future in order to assess a car's safety.